

High-Resolution Wind Fields within the Inner Core and Eye of a Mature Tropical Cyclone from GOES 1-min Images



A. F. Hasler,* K. Palaniappan,† C. Kambhammetu,‡
P. Black,§ E. Uhlhorn,§ and D. Chesters§

ABSTRACT

Mesoscale wind fields have been determined for a mature hurricane with high spatial and temporal resolution, continuity, and coherency. These wind fields, near the tropopause in the inner core and at low levels inside the eye, allow the evolution of mesoscale storm features to be observed. Previously, satellite-derived winds near hurricanes have been determined only at some distance from the eye over a typical time period of 1–2 h. Hurricane reconnaissance aircraft take 30 min to 1 h to complete an inner-core pattern. With the long observation periods of these previous methods, steady-state conditions must be assumed to give a complete description of the observed region.

With the advent of 1-min interval imagery, and fourfold improvement of image dynamic range from NOAA's current generation of GOES satellites, there is a new capability to measure inner-core tropical cyclone wind fields near the tropopause and within the eye, enabling mesoscale dynamical processes to be inferred. These measurements give insights into the general magnitude and structure of the hurricane vortex, along with very detailed measurements of the cloud-top wind's variations in response to convective outbursts. This paper describes the new techniques used to take advantage of the GOES satellite improvements that, in turn, allowed the above innovations to occur.

The source of data for this study is a nearly continuous 12-h sequence of 1-min visible images from NOAA *GOES-9* on 6 September 1995. These images are centered on Hurricane Luis with maximum winds of 120 kt (CAT4) when it was 250 km northeast of Puerto Rico. A uniform distribution of long-lived cirrus debris with detailed structure is observed in the central dense overcast (CDO), which has been tracked using the 1-min images. The derived wind field near the tropopause at approximately 15 km in the CDO region has a strong closed circulation with speeds up to 25 m s^{-1} , which pulses in response to the convective outbursts in the eyewall. Cloud displacements are computed at every pixel in every image, resulting in a quarter-million $u-v$ winds in each of 488 hurricane images observed at 1- to 4-min intervals over 12 h. For analysis and presentation, these ultradense wind fields are reduced to 8- or 16-km grids using a 7-min time base by smoothing displacement vectors in space and time.

Cloud structures were tracked automatically on a massively parallel processing computer, but with manual spot-checking. Manual tracking has been used to follow CDO structure over long time periods, up to 90 min for a small test sample. Cloud tracking for the wind fields presented here is accomplished using a Massively Parallel Semi-Fluid Motion Analysis (MPSMA) automatic technique. This robust deformable surface-matching algorithm has been implemented on the massively parallel Maspar supercomputer. MPSMA automatic tracking typically follows a feature for 7 min. For this time base the error of these winds is estimated to be 1.5 m s^{-1} . However, systematic navigation and height assignment errors in the moderately sheared hurricane environment must still be considered. Spatial and temporal smoothing of the wind field have been performed to reduce systematic navigation errors and small-scale turbulent noise. The synthesis used here to compute the wind fields gives an order of magnitude reduction in the amount of data presented compared to the amount of data processed. Longer tracking could give higher accuracy but would smooth out the smaller-scale spatial and temporal features that appear dynamically significant.

The authors believe that the techniques described in this paper have great potential for further research on tropical cyclones and severe weather as well as in operational use for nowcasting and forecasting. United States and foreign policymakers are urged to augment the GOES, GMS, FY2, and Meteosat geostationary satellite systems with dual imaging systems such that 1-min observations are routinely taken.

*NASA/Goddard Space Flight Center, Greenbelt, Maryland.

†Department of Computer and Information Science, University of Delaware, Newark, Delaware.

§Hurricane Research Division, NOAA/Atlantic Oceanographic and Meteorological Laboratories, Miami, Florida.

‡Laboratory for Atmospheres, NASA/Goddard Space Flight Center, Greenbelt, Maryland.

Corresponding author address: Dr. A. Frederick Hasler, NASA/Goddard Space Flight Center, Code 912, Greenbelt, MD 20771.
In final form 16 June 1998.

©1998 American Meteorological Society

1. Introduction

Even before the advent of the *Advanced Technology Satellite-1*, the first geosynchronous weather satellite in 1996, it was speculated that clouds could be used like free weather balloons to estimate atmospheric winds. Early measurements include those of Fujita et al. (1968), Hasler (1970, 1972), Hubert and Whitney (1971), and Young et al. (1972), and automated methods of estimation include those of Leese et al. (1971) and Smith and Phillips (1972). Errors associated with wind measurements made in conjunction with in situ aircraft wind verification (Hasler et al. 1979) were reported based on a series of experiments that confirmed the accuracy and utility of cloud winds. Errors were reported on the order of $1.5\text{--}2 \text{ m s}^{-1}$, which are as good as the measurement accuracy associated with rawinsonde winds.

Recently Velden et al. (1997) have improved the concept of satellite-derived winds by developing new techniques for estimating water vapor winds and by showing that wind fields derived from multispectral imagery have a positive impact on global and regional circulation model forecasts. Wind vectors derived from cloud motions are part of data assimilation used for regional forecast systems in the United States (Merrill et al. 1991; Nieman et al. 1996) and Europe (Erikson 1990). Hasler and Morris (1986), Velden et al. (1992), Velden et al. (1998), and Goerss et al. (1998) have shown that satellite-derived winds can also be used effectively for hurricane studies. However, with the 15–30-min image intervals available in the past, it has been impossible to measure winds near and in the hurricane eye region. The only features in the central dense overcast (CDO) that can be tracked at 15+ min intervals are deep convective towers that cannot be used to estimate winds at cloud top. Current methods of wind measurement in hurricanes include the following:

- NOAA WP-3D and U.S. Air Force Reserve (AFRES) WC-130 aircraft, which traverse storms usually in a crossing alpha pattern;
- dropsondes from the WP-3D flying at up to 5-km altitude or the new National Oceanic and Atmospheric Administration (NOAA) Gulfstream G-IVSP flying at up to 12-km altitude;
- occasional routine or special rawinsondes that are launched through a passing tropical cyclone, or surface buoys that report observations every 10 min to 1 h as the storm moves by;

- ground-based Next-Generation Radar or airborne Doppler radar observations using the tail radar of the WP-3D; and
- satellite-derived winds (Hasler and Morris 1986; Velden et al. 1992; Velden et al. 1998) outside the cyclone CDO area.

In all of these methods, the storm is assumed in steady state over the observation period, which can vary from 1.5 h for an aircraft flight-level pattern to 6–8 h for a dropsonde pattern to as much as 24 h for storm sampling by buoys and rawinsondes. Kidder and Vonder Haar (1995) reviewed most of these wind estimation methods.

The current generation of geostationary satellites [NOAA (*GOES-8, -9, -10*)], producing images with high spatial, temporal, radiometric, and spectral resolution (Menzel and Purdom 1994), and the use of improved automatic cloud-tracking algorithms allow investigation of mesoscale atmospheric phenomena such as hurricanes and severe convective storms. Geostationary Operational Environmental Satellite (GOES) imager superrapid scan sequences of mature hurricanes at 1-min intervals give new capabilities to observe tropical cyclone dynamics. Detailed cloud structure can now be seen in most areas of the CDO due to the good contrast in spite of very bright clouds. The 1-min interval between images allows features to be tracked with accuracy and reliability. During the checkout phase of the NOAA *GOES-9* satellite a unique nearly continuous 12-h sequence of 1-min images of Hurricane Luis on 6 September 1995 was obtained. A uniform distribution of long-lived cirrus debris structure with detailed structure has been found in the CDO. The debris has been tracked over long periods, up to 90 min, in most regions of the CDO.

Systematic errors associated with older, lower time resolution visible imagery obtained at 30- and 60-min intervals are primarily due to the difficulty in tracking cloud elements over longer time intervals and poor height assignment. The difficulty in automatically tracking cloud elements over long time intervals is a result of strong deformation fields, evaporation and formation of individual elements, and vertical shear. For high time resolution imagery the problem of tracking distinct elements across adjacent images is almost nonexistent; however, automatically estimating a dense wind field with deforming cloud structures throughout the image, as shown in Fig. 1, is an extremely challenging task (Palaniappan et al. 1996). The increased dynamic range imager data (10 bits vs 6 bits

in earlier GOES satellites) allows for much improved performance in tracking deforming cloud surface features. However, the accuracy in computing dense wind fields is reduced unless longer image sequences are used and the height assignment problem can be addressed using stereo image sequences (Palaniappan et al. 1995).

The paper is organized as follows: section 2 describes techniques for automatic cloud tracking, verification, error analysis, wind field noise reduction by smoothing, and cloud-height assignment; section 3 describes the results in terms of high-level, midlevel, and low-level derived wind fields and the interpretation of these fields; and section 4 gives conclusions, recommendations, and describes work in progress and future work.

2. Techniques

a. The MPSMA automatic technique for cloud feature tracking

Correlation-based methods for automatic cloud tracking were pioneered by Leese et al. (1971) and improved by Smith and Phillips (1972) and Phillips et al. (1972), and generally provide satisfactory results for tracking well-identified isolated cloud tracers. The underlying assumption of correlation-based methods is that the feature or object being tracked moves rigidly, that is, without deformation. However, within the CDO of a hurricane or severe storm more general methods for automatic cloud tracking need to be developed to accommodate cloud deformations and the complex behavior of multilayered cloud surfaces. A robust method of automatic cloud surface tracking under nonrigid deformations has been developed to determine a dense wind field as described by Palaniappan et al. (1995) and Palaniappan et al. (1996). The deformable motion estimation algorithm has been implemented on a fine-grained massively parallel Maspar MP-2 supercomputer with 16 384 processor elements to track every pixel in the image. We henceforth refer to this as the Massively Parallel Semi-Fluid Motion Analysis (MPSMA) automatic technique.

A deformable motion model is a more realistic representation of the dynamics of cloud surfaces that relaxes the rigid motion assumption typically used in optical flow field methods for the estimation and segmentation of dense motion vectors (Huang et al. 1995). A nonrigid motion model enables the automatic tracking of a dense set of uniformly distributed tracers in

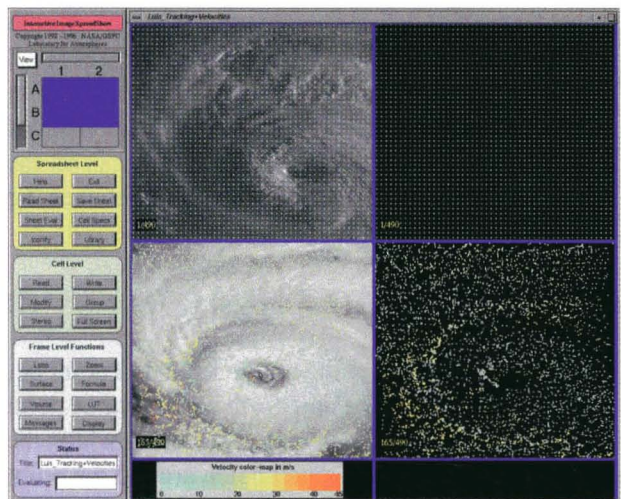


FIG. 1. Tracer positions using the MPSMA automatic cloud tracking technique with computation from a massively parallel processing computer. In the top row of the IISS cells, every 10th pixel is marked at the beginning of the tracking period. In the bottom row, the position of the features is shown after tracking every minute for a period of 4 h. In the first column of cells, the cloud tracers are overlaid on the GOES image at the corresponding time. Weightless tracers are colored according to their speed as given in the legend.

the cloud motion vector field. Two successful approaches were developed by Palaniappan et al. (1995), Palaniappan et al. (1996), and Kambhamettu et al. (1996) to characterize the deformation of cloud surface pixel arrays and model the complex dynamics of clouds exhibited in the CDO region and in regions of multilayer cloud decks. The first approach uses a *continuous motion model*, where individual cloud elements are assumed to undergo locally continuous deformation (i.e., the cloud surface patch can be smoothly stretched with local elements maintaining their neighborhood relationships). The second approach uses a *semifluid motion model*, where the local continuity constraint may be violated during deformation. The semifluid model allows cloud surface patches to merge, split, or cross over but is computationally more expensive and requires more careful selection of matching parameters. These methods are briefly described below.

For automatic nonrigid motion analysis of cloud imagery at short time intervals, a local small deformation assumption can be used to derive relationships between unit normals and surface curvatures of a point on the surface before and after motion. A more detailed description of the derivation and algorithm used for the MPSMA automatic technique is found in Palaniappan et al. (1995) and Palaniappan et al. (1996).

Consider a point defined parametrically as $z(x, y)$, with unit normal vector \mathbf{n} , on a surface that undergoes small deformation changes and is transformed to the point $z'(x', y')$. The normal vector \mathbf{n} is a unit vector perpendicular to the tangent plane at the point $z(x, y)$ on the surface. The following relationship holds between the corresponding unit normals:

$$\mathbf{n}' = \mathbf{n} - \mathbf{n} \times \text{rots}, \quad (1)$$

where \mathbf{n} corresponds to the unit normal of a point before motion and \mathbf{n}' is the unit normal of the same point after motion. The nonrigid motion occurring within the local neighborhood of a small patch around the point of interest can be expressed in the imaging instrument coordinate system at the initial time step as

$$\mathbf{s} = [x' - x, y' - y, z'(x', y') - z(x, y)], \quad (2)$$

where \mathbf{s} models the displacement function. The rotation or *curl* of the displacement function or motion field will be denoted by $\text{rot } \mathbf{s}$ and can be shown to be

$$\text{rot } \mathbf{s} = \frac{1}{E} \frac{\partial z}{\partial x} \times \frac{\partial s}{\partial x} + \frac{1}{G} \frac{\partial z}{\partial y} \times \frac{\partial s}{\partial y}, \quad (3)$$

which requires partial derivatives of the surface and the displacement function with respect to the parameters x and y , respectively. The denominators are given by

$$E = 1 + \left(\frac{\partial z}{\partial x} \right)^2, \quad G = 1 + \left(\frac{\partial z}{\partial y} \right)^2 \quad (4)$$

and are the coefficients in the first fundamental form, which is used to measure metrical properties of surfaces including lengths, angles between curves, and areas on the surface $z(x, y)$. Surface normals and other intrinsic surface properties are estimated by using locally fitted quadratic surfaces.

Polynomial functions are the simplest models for the local displacement function of a small patch undergoing small deformation. In our cloud motion experiments, and in order to derive simple analytical relationships for differential geometry parameters, a small patch is assumed to undergo a local affine transformation. The components of the displacement function, $\mathbf{s}(\bullet)$, are the unknowns that are solved. Since each small patch is assumed to experience small deforma-

tions locally, this constraint is used to hypothesize a set of point correspondences or equivalently a template mapping, η_R , over a small search area between corresponding cloud surface patches at the two different time steps. The error function is then minimized with respect to each of the unknowns. Using the estimated displacement function associated with each hypothesis the errors $\varepsilon_R(x, y)$ are ranked. The hypothesis associated with the smallest error is used as an estimate of the local cloud motion vector. In the semifluid motion model, the intensity information for each local patch is utilized to determine a set of possible semifluid template mappings. The error matching then selects the most reliable semifluid mapping.

The MPSMA automatic technique incorporates both the semifluid and continuous motion models, which led to a performance speed up of between 1000 and 300 times, respectively, in comparison to the sequential version of the semifluid motion analysis algorithm running on an SGI workstation with an R8000/90-MHz CPU. The parallel implementation becomes a necessity when analyzing a long sequence of images, such as the 488-frame Hurricane Luis visible image sequence. Estimating a dense wind field using a deformable motion model requires about 10 min per pair of images over a 512×512 pixel domain, versus about 40 h per pair of images using the sequential implementation. Figure 1 illustrates the results of automatic cloud tracking visualized using the Interactive Image SpreadSheet (IISS) (Hasler et al. 1994). The upper two cells mark every 10th pixel at the beginning of the tracking period; the elements can be considered as weightless particle tracers injected into the wind field. In the lower two cells the position of the particles or cloud surface pixel areas is shown after tracking them every minute for a period of 4 h. This shows the capability of tracking evolving features continuously over long periods. The color of the tracers is related to the instantaneous local wind velocity scaled in meters per second.

Though most of the 12-h sequence of Luis images has 1-min intervals, there are some discontinuities in the sequence. We have used the parameters shown in Table 1 in our automatic cloud tracking.

b. Time interval versus accuracy of cloud tracking

Using only one pair of images covering a brief time interval would result in the most dense wind field estimate covering the most clouds (essentially at every grid point or pixel) This would give high confidence that few feature matching mistakes were

TABLE 1. Size of the template (original pixel domain) and search area (second domain over which the template is matched) in the automatic tracking as a function of time interval.

Time interval (min)	Template	Search area
1	11 × 11	15 × 15
2	15 × 15	22 × 22
3	17 × 17	26 × 26
4	19 × 19	29 × 29

made. However, the wind field would have very low accuracy. To improve the accuracy of the estimated wind vectors a longer time interval is required over which the same cloud patch needs to be tracked. If a longer time interval is used, the baseline accuracy of the wind velocity increases but the number of clouds tracked decreases, due to finite cloud lifetimes.

The resolution of the current NOAA GOES images is 1 km (with an oversampling factor of 1.75 in the east–west x direction). Images are resampled in the x dimension to give the proper aspect ratio. If it is assumed that the error in the position location of a sample is 1 km, then the solid line in Fig. 2 gives the theoretical motion measurement error as a function of time interval. If random errors of 1-km rms are added to the x and y coordinates of each data point, the resulting errors are given as the dashed line in Fig. 2.

Errors of 1 m s^{-1} or less in the motion measurement are considered to be an excellent level of accuracy. From Fig. 2, it is seen that a 10-min time base is needed to achieve approximately a 1 m s^{-1} wind error in the presence of one-pixel random location errors. Winds obtained from a 1-min time base would have an unacceptable error of 9.7 m s^{-1} . Fortunately, a large number of the clouds in the CDO that we are tracking have lifetimes of 7–15 min or longer. In fact, one cloud that was manually tracked had a lifetime of 90 min as described below in Fig. 3.

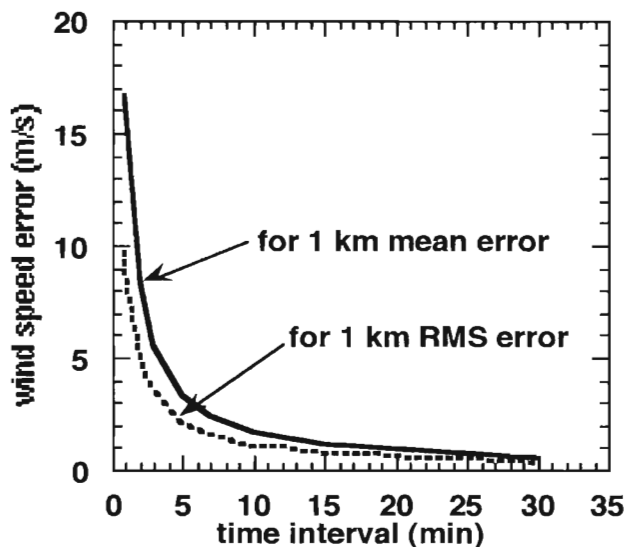


FIG. 2. Cloud-tracked motion measurement error as a function of time interval for 1-km mean or 1-km rms position errors. If a random error of one-pixel rms is added to the x and y coordinates of each data point, the resulting errors are given as a function of the length of time a cloud is tracked.

c. Manual cloud tracking

IISS (Hasler et al. 1994) was used to track clouds in the CDO appearing in as many as 80 images over 90 min as shown in Fig. 3. Cubic spline smoothed curves are fit to the manually determined trajectories. Speed is calculated by using the length of the fitted curve and direction given by the tangent at any point. The ability of tracking cloud features over these long periods was instrumental in convincing the authors that the features followed are relatively con-

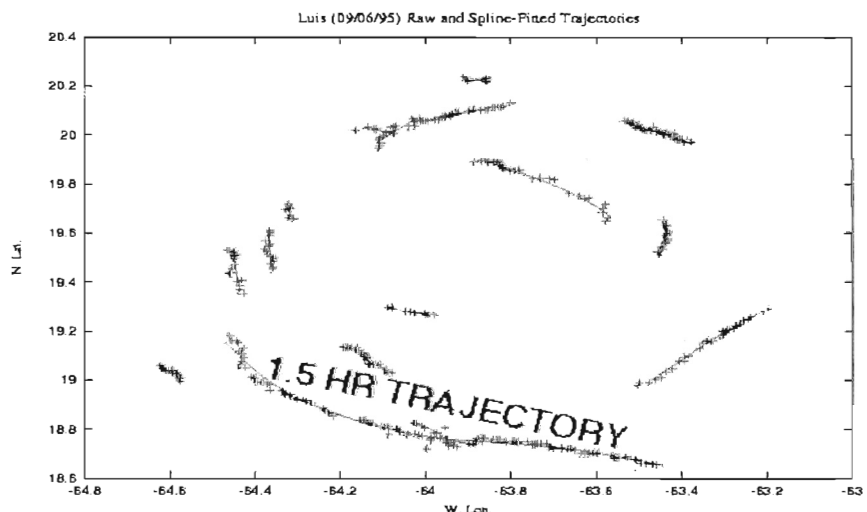


FIG. 3. Manually tracked clouds near the tropopause in the CDO of Hurricane Luis from 1-min interval GOES-9 images, showing cloud lifetimes of up to 90 min.

servative cirrus debris, which make excellent cloud wind tracers.

d. Calculation of winds

Output from MPSMA automatic cloud-tracking technique consists of 512×512 grids of row and column pixel shifts. That is, the displacement of each pixel across images adjacent in time is given as two integers, one representing the column displacement (i) and the other the row displacement (j). With satellite navigation data providing the latitude-longitude of each pixel the derivative may be computed and thus the u and v components of the wind field.

With a series of 488 visible images spanning a time period of approximately 12 h the computation of the winds using high-order finite-difference schemes becomes possible. For the first-order truncation error method the horizontal components in the image coordinate system wind at a point (i,j) is just

$$u = \frac{dx_{i,j,t}}{dt} = \frac{(i + \Delta i, j)_{t+\Delta t} - (i, j)_t}{\Delta t},$$

$$v = \frac{dy_{i,j,t}}{dt} = \frac{(i, j + \Delta j)_{t+\Delta t} - (i, j)_t}{\Delta t}, \quad (5)$$

where u and v are the wind components, along rows and columns, respectively, and subscripts i and j are the pixel shifts in the i and j directions, respectively. The above constitutes a forward finite-differencing scheme. For schemes of order two and higher, centered difference methods may be used. The order two scheme computes derivatives from positions forward one time step ($t + \Delta t$) and backward one time step ($t - \Delta t$). The fourth-order method uses positions twice forward in time and twice backward, and so on. For purposes of error analysis, winds are computed using finite-difference methods up through the eighth-order truncation error, which requires four forward and four backward positions to compute the derivative. In theory, methods of higher order yield more accurate results. In practice, the high-order derivatives of experimental observations usually suffer when differences are small. Indeed, the errors for this particular application reach a minimum for the second-order calculation and increase for higher-order methods. This is believed to be due to computing derivatives across discontinuities in the automatic wind tracking

data. Errors for each scheme are shown in Fig. 4 and may be compared with the theoretical error for a time base of 1 min shown in Fig. 2. The errors shown in Fig. 4 are based upon a 1-min time base for each order of finite-difference approximation used. Errors in wind speed are given in meters per second by adding a random value of zero mean and unit variance of pixel displacement to each end point of each of the automatically determined cloud trajectories. Thus approximately 68% (one standard deviation) of the endpoints are in error by less than one pixel (~ 1 km) and the remaining 32% are in error of magnitude greater than one pixel.

Based on results of the error analysis for each scheme, the second-order method has been chosen. Using this method a series of 488 gridded wind fields of resolution equal to the original data is computed.

e. Noise reduction

As described previously there are numerous sources of error that contaminate the wind fields produced by the automatic cloud-tracking algorithm. In addition to noise associated with these errors, a great deal of noise associated with meteorological phenomena is generated. The trajectory of an individual cloud element is a result of the sum of motions across several scales in time and space. This includes the interaction of motions at the smallest turbulent scales with

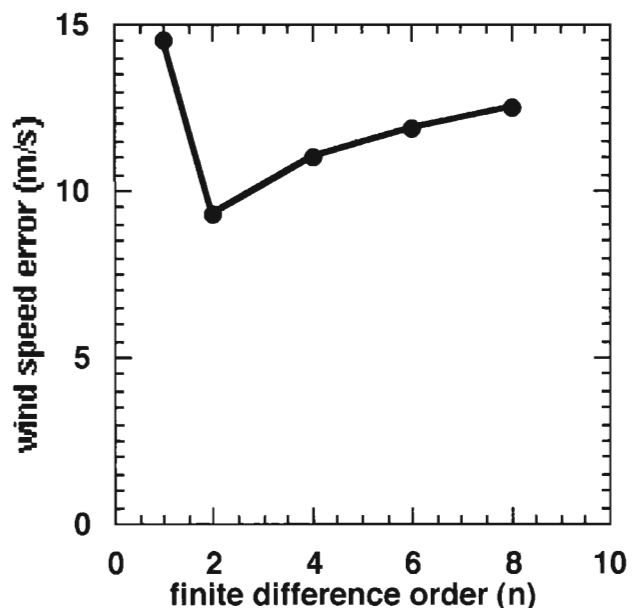


FIG. 4. Cloud motion measurement error, as a function of order of truncation error, for a time base of 1 min. The centered difference of order two is most accurate and significantly decreases the error in computing winds over a first-order difference.

synoptic-scale flow. Other motions visible in the imagery include internal waves excited by unstable regions of the atmosphere that do not necessarily contribute to the wind field.

To accurately analyze a synoptic wind field such as a hurricane-scale vortex and to be able to resolve mesoscale circulations embedded within the storm, high-frequency and short-wavelength data must be in some way separated or removed altogether. Also, wave motions seen by the automatic algorithm as contributing to the displacement of a pixel (cloud element) should be deleted as well. Removal of this information must be performed while leaving the relevant wind data intact. In other words, what is desired is a smoothed wind field without damping significant wind structure.

For purposes of this research, a noise removal method based on the fast Fourier transform (FFT) is used. The Fourier transform attempts to represent a function in terms of an infinite series of complex trigonometric functions or modes. Each mode corresponds to a particular frequency, and the amplitude of each mode represents the energy. The energy contained at particular wavebands may be damped or completely removed by application of a filter function to the spectral data. The Fourier transform is an invertible linear operation and can, therefore, be used to return the filtered spectral data to a real domain (i.e., time or space), yielding a filtered (smoothed) dataset. The amount of smoothing was determined by trial and error to give minimal damping of coherent wind field structure.

The automatically computed winds are 512×512 datasets of u and v components at each time in the series of visible images. First the short-wavelength noise is removed via application of the fast Fourier transform algorithm based on the method of Rybicki (Press et al. 1992), in conjunction with a filter function. The two-dimensional FFT is used to compute the energy spectrum as a function of wavenumber for each image in the series. The filter function applied to the transformed data is a unit step such that all components of wave-

length longer than a specified value are multiplied by one. All others are multiplied by zero. This is a simple low-pass filter. The resulting energy spectrum is then submitted to the inverse FFT routine to return the original dataset without high-frequency components. Next, the spatially filtered data is passed to a one-dimensional FFT time-domain routine for purposes of filtering high-frequency information. A low-pass filter similar to the spatial case is then applied to the time series of data. All energy of higher frequency than a specified value is removed, the inverse FFT is computed, and a both spatially and temporally filtered gridded wind dataset results. Therefore it is not surprising that the wind fields show great temporal and spatial continuity.

The synthesis used here to compute the wind fields produces an order of magnitude reduction in the amount of data presented compared to the amount of data processed. Eight temporal measurements over 7 min are made on a 1-km grid, but the results are

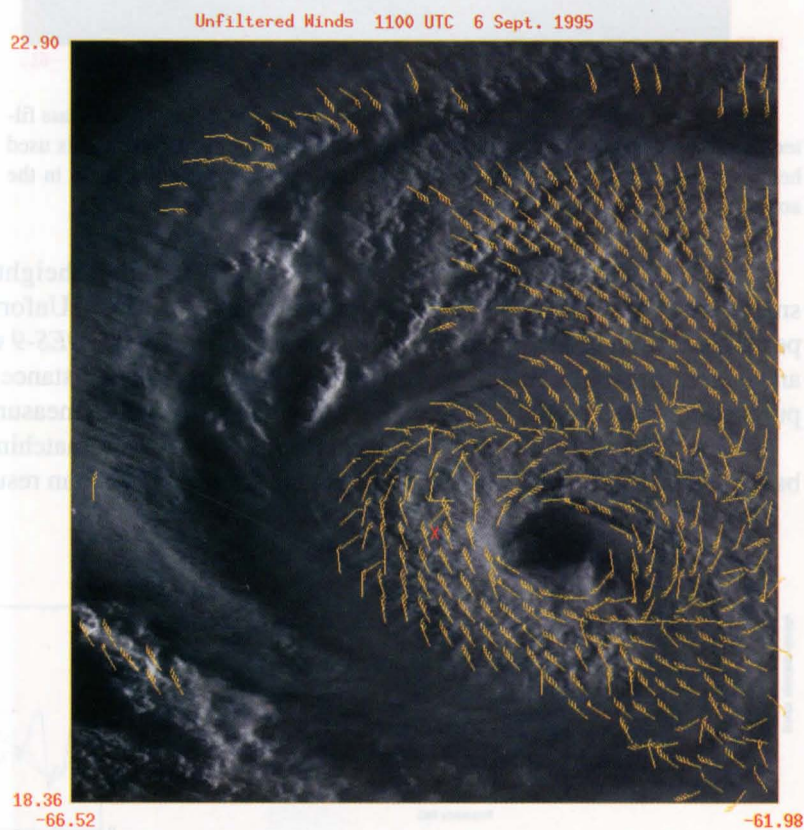


FIG. 5. Hurricane Luis inner-core winds at an altitude of 15 km using the MPSMA automatic cloud tracking technique at 1100 UTC prior to use of low-pass filter. The orange "X" near the center of the image corresponds to the location of a corresponding power spectrum plot shown in Fig. 7 and to a corresponding time series plot of wind speed shown in Fig. 8. Wind barbs are plotted at every 16th pixel.

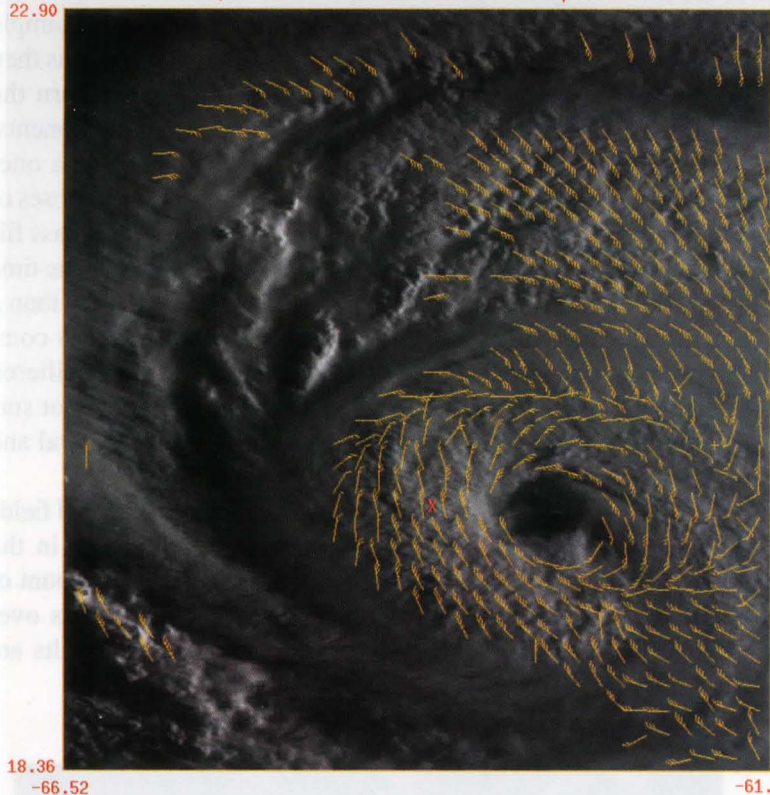


FIG. 6. Same as Fig. 5 after low-pass temporal and spatial filtering. Low-pass filter cutoffs are wavelength $L = 100$ km and period $T = 65$ min. The synthesis used here to compute the wind fields produces an order of magnitude reduction in the amount of data presented compared to the amount of data processed.

smoothed to a 16-km grid. The 7-min measurement period is chosen as a compromise between accuracy and temporal resolution. The 16-km grid is chosen for purposes of presentation clarity.

Figure 5 shows unfiltered winds from a 7-min time base plotted on the 1100 UTC GOES visible image

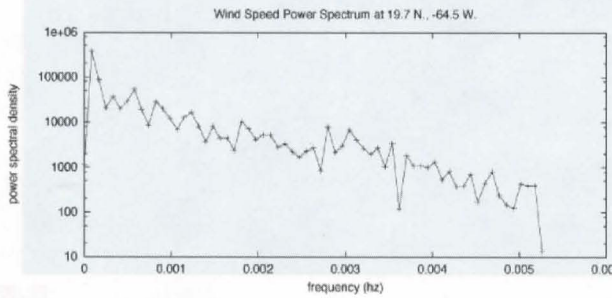


FIG. 7. Power spectral density (PSD) as a function of frequency (Hz) for grid point 19.7°N , 64.5°W (denoted by orange X in the wind field plots in Figs. 5 and 6) for output from automatic algorithm. The low signal-to-noise ratio (seen by the slow decrease in the PSD with increasing frequency) necessitates application of spectral filters in order to obtain a relatively noise-free wind field.

prior to application of low-pass spatial and temporal filters.

Figure 6 shows a plot of filtered winds after low-pass temporal and spatial filtering. Note that small-scale turbulent features and systematic noise have been smoothed out.

Figure 7 shows the power spectral density (PSD) as a function of frequency (Hz) for the grid point near the eye of Hurricane Luis.

Figure 8 shows a time series of wind speed at the same location as the PSD in Fig. 7 over a period of 2 h from 1020 to 1220 UTC on 6 September 1995. The mesoscale variability and larger features remain while the high-frequency signal (noise) is removed in the filtering process.

f. Wind height assignment

Stereo measurements from GOES-8 and -9 were available at 15-min intervals during the day on 6 September 1995. A parallel automatic stereo analysis algorithm was used to estimate heights of the CDO in Luis using coincident stereo pair imagery (Palaniappan et al. 1995; 1998). The

stereo heights are estimated to be approximately 15 km. Unfortunately in September of 1995 GOES-8 and GOES-9 were separated by only 15° of longitude. That distance provides a relatively short baseline for stereo measurements.

A matching error of one pixel in the region of the CDO can result in an error in the stereo cloud height

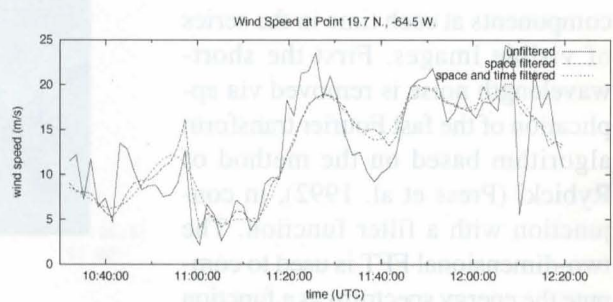


FIG. 8. Time series of wind speed at same location as the PSD in Fig. 7. The three plots are for the 1) unfiltered wind speed, 2) wind speed after spatial filtering, and 3) wind speed after spatial and temporal filtering.

assignment of about 1.5 km, which explains why it has been impossible to detect variations in height across the CDO. The Doppler tail radar from the NOAA P3 puts the top of the CDO in the eyewall region at 13.9–16.6 km. The San Juan rawin soundings at 0000 UTC on 6 and 7 September 1995 clearly show the tropopause at 150 Mb (14.2 km). The tropopause is less well defined at 1200 UTC 6 September 1995 but is not inconsistent with that number. It is well known that the tropopause bulges upward over a mature hurricane. The heights obtained from the stereo and Doppler measurements would indicate an upward bulge of about 1 km.

Weaker convective cells will top out at the tropopause and stronger ones will overshoot as far as 2 km into the stratosphere. During the period of the dataset presented here the overshoot was moderate and most likely did not exceed 1 km. For the purpose of model height assignment, 15 km appears to be a good height to use, but there are most likely variations in the height of the winds on the order of ± 1 km across the CDO that cannot be resolved.

3. Results

A 2-h superrapid scan subset of a 12-h GOES-9 imager visible image sequence for Hurricane Luis has been processed automatically to determine an ultradense time-varying wind. As described in section 2, the MPSMA automatic technique incorporates deformable motion modeling for matching cloud surface pixel arrays and is capable of tracking cloud pixel arrays for their complete lifetime. However, the dense wind field produced by the semifluid motion analysis algorithm contains outliers due to registration errors in the image sequence. A low-pass filter was applied to smooth the resulting wind fields both spatially and temporally. The smoothing was very effective at reducing systematic errors due to scan-to-scan and image-to-image misregistration errors.

Figure 9 shows wind field vectors derived by the automatic method at 1104 UTC

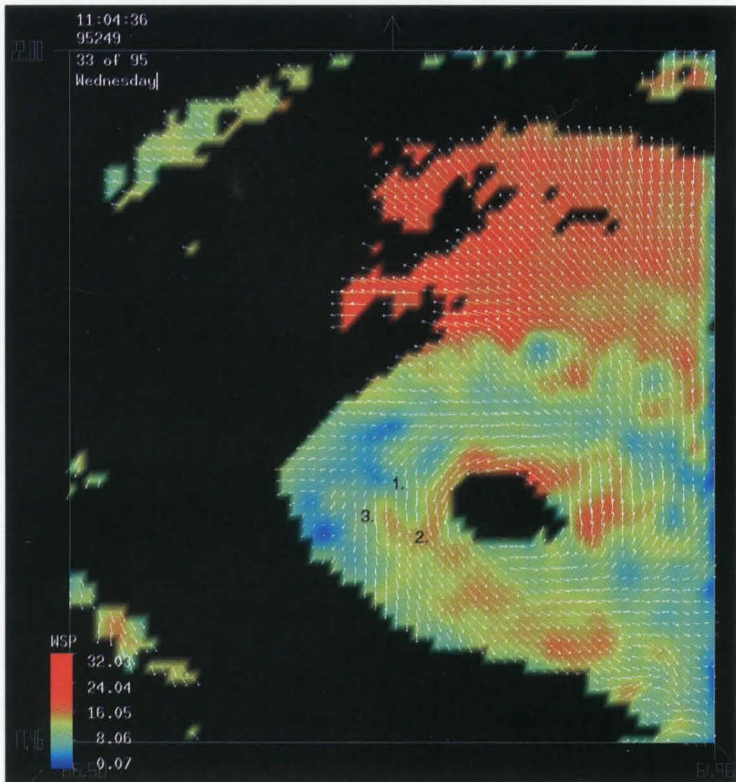


FIG. 9. Luis 15-km inner-core winds using the MPSMA automatic cloud tracking technique, 1104 UTC, 8-km grid; see legend for wind speed colors.

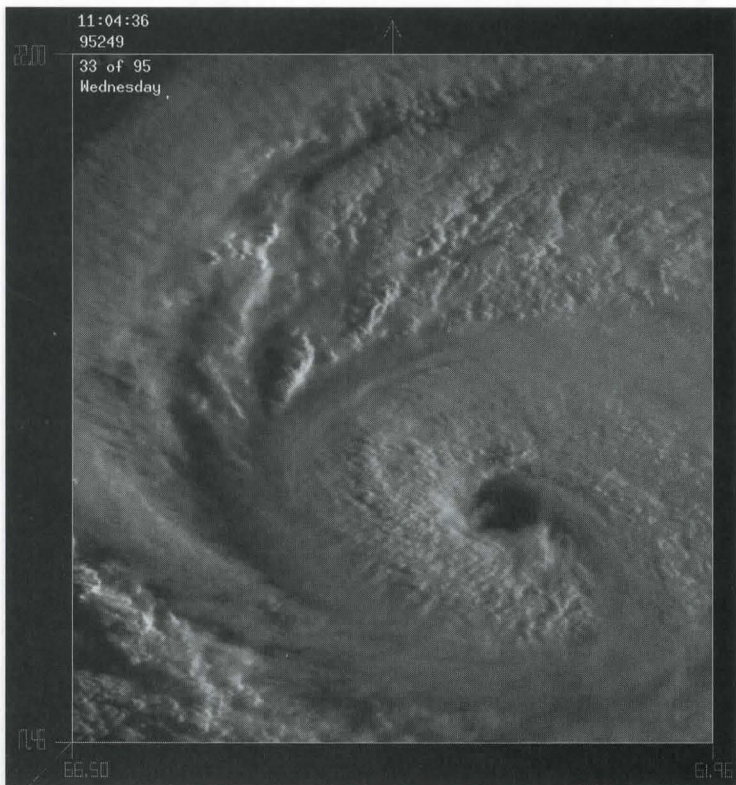


FIG. 10. NOAA GOES-9 visible image at 1104 UTC 6 Sep 1995 at the same time as the wind field shown in Fig. 9.

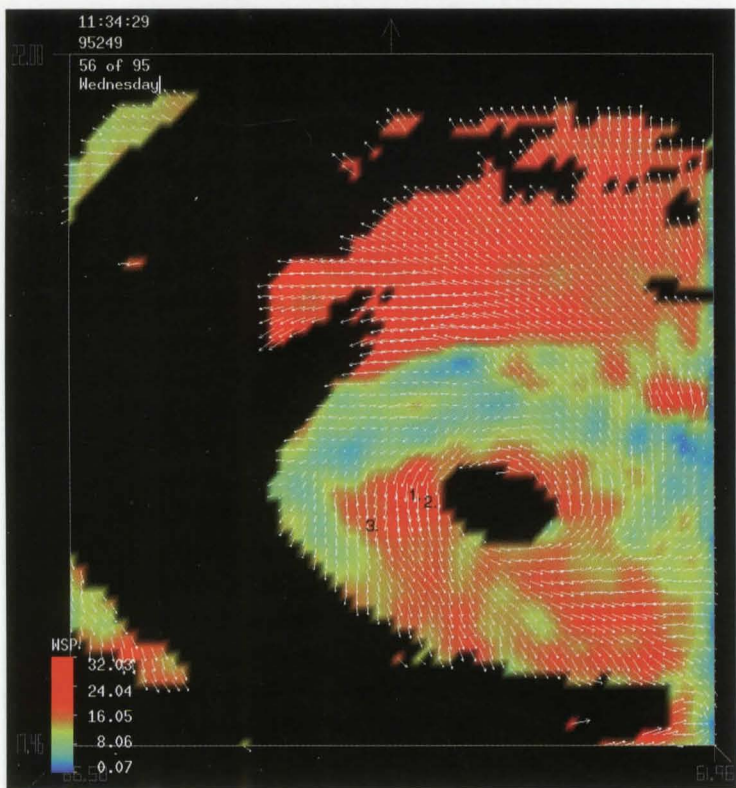


FIG. 11. Same as Fig. 9 except at 1134 UTC. Note the dramatic increase in wind speed west and south of the eye.

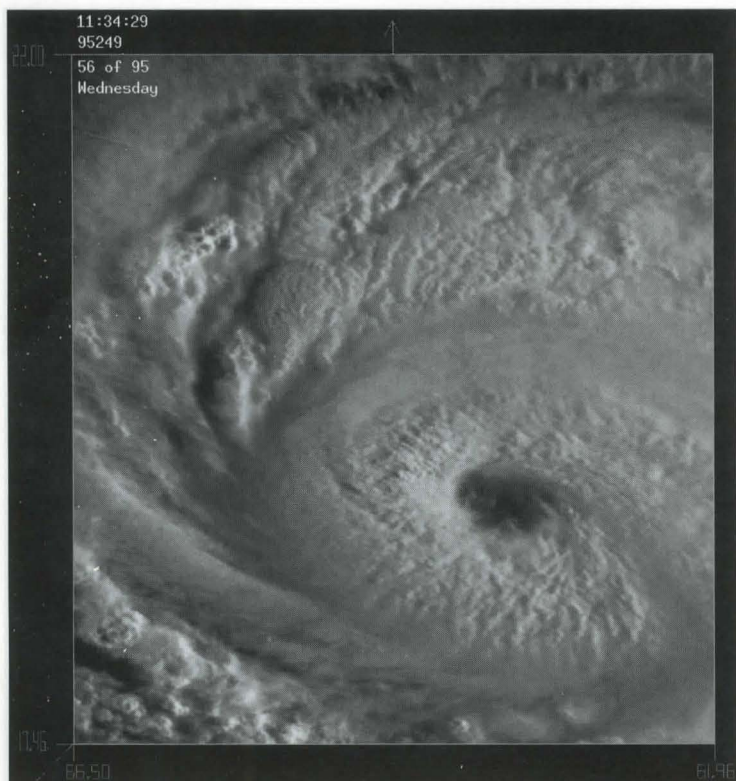


FIG. 12. NOAA GOES-9 visible image at 1134 UTC 6 Sep 1995 at the same time as the wind field shown in Fig. 11.

6 September 1995 with wind speed given as a color lookup table as shown in the legend. Highest wind speeds are shown in red and lowest in blue. Note the wind speeds at locations 1, 2, and 3 are given as 11.5, 14.6, and 7.7 m s^{-1} , respectively. Figure 10 shows the *GOES-9* visible image at the same time as Fig. 9. Figure 11 shows the wind field 30 min later at 1134 UTC 6 September 1995 with the same units as Fig. 9. Note how the wind speed has dramatically increased west and south of the eye. This is particularly dramatic at locations 1 and 3, where the wind speeds have increased from 11.5 to 22.8 m s^{-1} and 7.7 to 16.6 m s^{-1} , respectively, over the 30-min period. Figure 12 shows the visible *GOES* image at the same time as Fig. 11. Note the convective outburst to the northwest of the eyewall in Fig. 12 that may account for the increase in wind speed west and south of the eye as illustrated in the differences between Figs. 9 and 11.

Hurricane Luis's low- and midlevel winds in the eye derived using the MPSMA automatic cloud tracking technique are shown in Fig. 13. This figure illustrates the high spatial and temporal resolution, which is feasible using the MPSMA technique with a long time series of 1-min *GOES* images. The figure presents a sequence of 19 wind fields with time intervals from 1 to 4 min beginning at 1104 and ending at 1134 UTC on 6 September 1995. The low-level wind barbs in green and midlevel wind barbs in yellow on an 8-km grid are superimposed on the NOAA *GOES-9* visible images. The automatic wind data are masked using the *GOES* 11- μm IR channel to separate low, mid-, and high levels. The brightness temperature values that were used were low-level brightness temperature (T_b) $\geq 265 \text{ K}$, midlevel $265 \text{ K} > T_b \geq 225 \text{ K}$, and high level $225 \text{ K} > T_b$. The depth of the boundary layer in the eye of a tropical cyclone is expected to be 300–700 m. According to previous studies by Hasler et al. (1984) we would expect to assign the low-level winds to the cloud-base level or approximately 500 m. Note the subtle motions of the circulation center shown by the

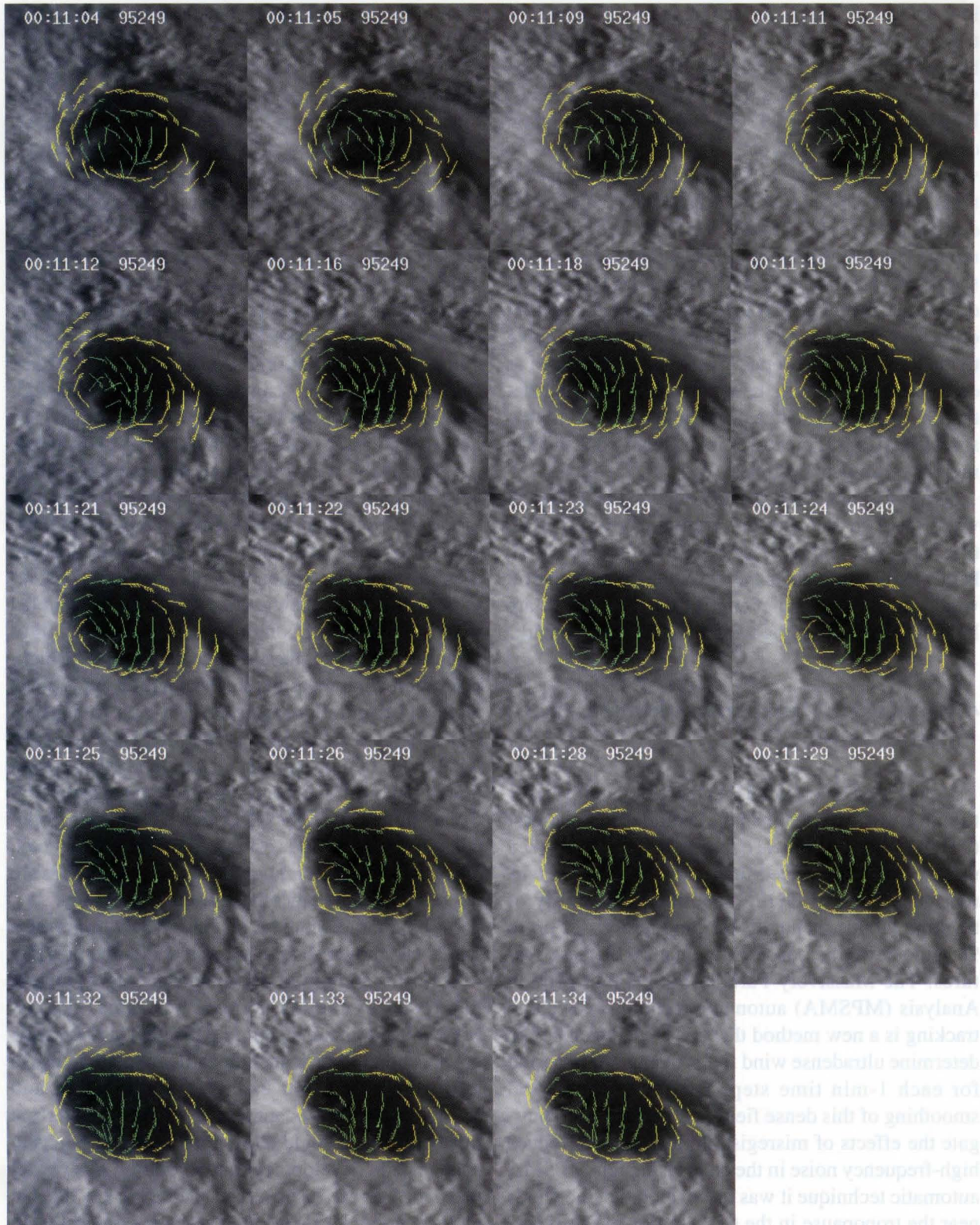


FIG. 13. Hurricane Luis low- and midlevel winds in the eye using the MPSMA automatic cloud tracking technique. A sequence of 19 NOAA GOES-9 visible images from 1104 to 1134 UTC 6 Sep 1995 is shown with low-level wind barbs in green and midlevel wind barbs in yellow superimposed. Note the high spatial and temporal resolution of the data.

low-level wind barbs in relationship to the center of the visible eye. At 1034 UTC (not shown) the circulation center is located quite far to the southwest of the visible eye, where it is hidden by the eyewall clouds. By 1104 UTC (see Fig. 13) a well-defined circulation center has moved to a point slightly to the west of the visible eye center. By 1116 UTC the circulation center has moved to the southwest again and is again hidden by the eyewall clouds. The circulation center remains in this position until the end of the sequence shown in Fig. 13 at 1134 UTC. Over the 12-h period of the Luis 1-min GOES image sequence the motion of the circulation center is being determined relative to the low-level and upper-level eye and is related to convective outbursts in the eyewall. It is expected that this analysis will lead to a better understanding of mesoscale dynamical processes in the inner-core and eye regions of tropical cyclones.

Note also that wind speeds found in the low-level wind field in the eye are frequently over 50 kt (25.7 m s^{-1}) [as high as 65 kt (33.4 m s^{-1}) at 1119 UTC], hardly the classic calm in the eye of the storm. Midlevel wind speeds on the inner edge of the sloping eye are lighter, seldom reaching the 50-kt (25.7 m s^{-1}) mark.

4. Conclusions, recommendations, and future work

It has been determined that there is a uniform distribution of cirrus debris in the central dense overcast (CDO) of mature tropical cyclones that can be tracked using contrast-enhanced images from NOAA's current generation of GOES satellites. The ability of tracking clouds manually for long periods of up to 90 min shows the conservative nature of these features. The Massively Parallel Semi-Fluid Motion Analysis (MPSMA) automatic technique for cloud tracking is a new method that has been developed to determine ultradense wind fields over a 7-min period for each 1-min time step. Spatial and temporal smoothing of this dense field was performed to mitigate the effects of misregistration errors and reduce high-frequency noise in the data. Using this MPSMA automatic technique it was discovered that the winds near the tropopause in the CDO region of Hurricane Luis on 6 September 1995 had a strong closed circulation with speeds of up to 25 m s^{-1} (additional information is available online at <http://rsd.gsfc.nasa.gov/users/hasler/luis>). This rotational field pulses in response to the convective bursts in the eyewall. The

error of the wind fields presented here is estimated to be 1.5 m s^{-1} from clouds that have been tracked for 7 min. However, the effect of an estimated height assignment error of 1.0 km has not been accounted for. Spatial and temporal smoothing of the wind field has been performed, which mitigates the systematic navigation errors and reduces small-scale turbulent noise. The synthesis used here to compute the wind fields produces an order of magnitude reduction in the amount of data presented compared to the amount of data processed. However, height assignment errors in the moderately sheared hurricane environment require further analysis. A dropsonde capability is being developed for the National Aeronautics and Space Administration's ER-2 aircraft, which flies at 20 km. The ER-2 dropsondes will be the first opportunity for *in situ* verification of the satellite-derived CDO winds.

Previously, with infrequent observations, it has been difficult to use satellite imagery to deliver one of the most obvious parameters, namely, wind measurements, with sufficient resolution and accuracy in the most dynamic region of a phenomenon. The authors feel that this new source of wind data coupled with high-powered computers and computer algorithms demonstrates the ability to make accurate high-resolution wind measurements using the upper-level clouds in mature hurricanes. The 1-min tropopause CDO region data reported in this study give accurate wind fields of high spatial and temporal resolution in one of the most important regions of the tropical cyclone. Furthermore, the CDO region is near the tropopause (~ 15 -km altitude estimated from satellite stereo analysis and Doppler radar for Luis), where winds are not observable by any other current technology.

With a large database of 1-min CDO tropopause winds taken over several years it should be possible to add substantially to our understanding of mature hurricane dynamics using algorithms like the MPSMA automatic technique. Insights into the critical question of hurricane intensification are likely to be forthcoming. For example, the location and strength of outflow channels can be determined from this data, which could allow forecasting of intensity change. The development and evolution of eyewall mesovortices can be observed. These are key links in understanding hurricane intensification processes. In this instance of a mature hurricane, the strong closed circulation extends from the surface all the way to the tropopause as manifested in the CDO tropopause winds. A large database of this kind of data may yield a better statistical correlation to surface winds for

mature hurricanes than the Dvorak technique (Dvorak 1984) now in use.

Combining these measurements in the inner-core and eye regions with the cloud and water vapor derived winds of Velden et al. (1998) in the outer regions will give a much improved view of tropical cyclones over a wide range of spatial and temporal scales.

In addition to the unique long sequence of 1-min NOAA GOES images of Luis, many other datasets have been processed and coregistered. Those data include airborne weather radar, Doppler radar, and wind data from the NOAA WP-3D and AFRES WC-130 that were in the eye later in the day on 5 September 1995 around 1600 and 1900 UTC. Wind fields from the MPSMA automatic technique for the later periods have also been processed. There were a number of stronger convective outbursts later in the day. It will be interesting to see how these outbursts affect the winds at the tropopause in the CDO region. Studies relating satellite observations of the convective outbursts (cloud-top outburst morphology, CDO tropopause winds, low-level winds in the eye, GOES-8/9 stereo heights, etc.) to the WP-3D and WC-130 aircraft data are in progress. Mesoscale Model Version 5 (MM5) 3D numerical model simulations of Hurricane Luis on $22 \times 11 \times 3$ km nested-grid scales have also been run. Currently the model storm is too shallow. It does not accurately reflect the strong closed circulation revealed by the satellite-derived CDO tropopause winds. The convective parameterization and boundary layer schemes are being modified to see if a more realistic storm can be simulated that matches the in situ and satellite observations.

Viewing hurricane animation sequences with image intervals ranging from 1 to 30 min like those during Guillermo, see Fig. 14, is very disconcerting for lay persons and experts alike. Furthermore, even the long Luis 1-min image sequence has numerous gaps from 2 to 4 min. Until now the lapse-dissolve technique used for bridging these gaps has been much

less than satisfactory. A morphing technique similar to those commonly used for special effects on commercial television has been used very effectively to bridge gaps up to 30 min in the Guillermo sequence. Morphing shows great promise in making continuous sequences for science and public outreach. However, the morphing technique used to date is extremely labor intensive. Output of the robust automatic cloud feature matching technique described here is being used as input to an automatic morphing technique that could be used operationally.

The nearly continuous 12-h sequence of images from the NOAA GOES-9 satellite of Hurricane Luis on 6 September 1995 used in this study is the *only* long duration sequence at 1-min intervals that has ever been taken of a mature tropical cyclone (see Fig. 14). Figure 14 shows a comparison of the following: 1) the long 1-min image sequence taken during the Hurricane Luis GOES-9 test in 1995; 2) special short 1-min sequences of Hurricane Guillermo obtained during GOES-9 normal operations in 1997; and 3) 15-min data of Hurricane Linda in 1997. The 15-min data of Linda are all that was obtained this past year of the strongest storm ever observed in the eastern Pacific.

The authors believe that the techniques described in this paper have great potential for further research on tropical cyclones and severe weather as well as in operational use for nowcasting and forecasting. United States and foreign policymakers are urged to augment the GOES, Geostationary Meteorological Satellite, FY2 (Feng-Yun-2B), and Meteosat geostationary satellite systems with dual imaging systems such that 1-min observations are routinely taken.

Acknowledgments. The authors would like to acknowledge Matt Easton, now a graduate student of Bill Gray at CSU, for making the first estimates of Hurricane Luis CDO tropopause winds in a senior undergraduate paper. The authors had been looking at the CDO cloud structure motions since our first movies of Luis were made on 6 September 1995. The authors were not originally convinced that the motions were good estimators of the

GOES imager scene frequency

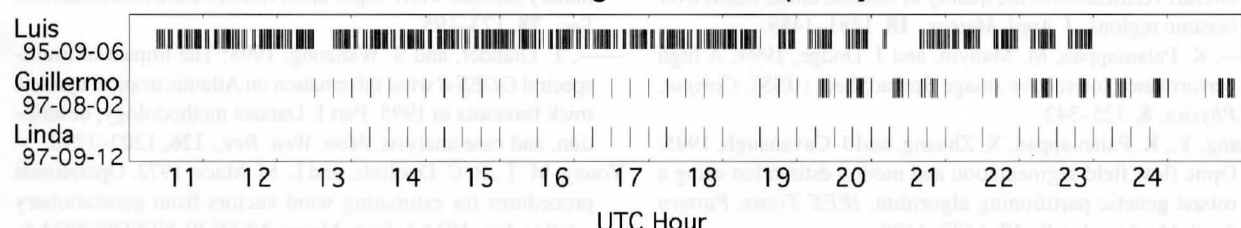


FIG. 14. NOAA GOES-9 image frequency for Hurricanes Luis, Guillermo, and Linda.

winds. However, once Matt Easton's results were presented and cloud tracks up to 90 min were obtained, it was apparent that an important new source of observations in mature hurricanes is at hand. Review of the manuscript with thoughtful suggestions by Mohan Karyampudi is greatly appreciated. The authors would like to thank Marit Jentoft-Nilsen and Hal Pierce for their work in processing the data for this study. The authors would also like to thank Jim Purdom and Joe Friday of NOAA for their support of the 1-min "rapid scan" NOAA GOES-9 operations. The development of the MPSMA automatic cloud tracking technique and IISS were supported under NASA grants, including NASA AISRP NRA-93-OSSA-09 for parallel motion analysis, NASA MTPE NRA-94-MTPE-02, NRA-94-OSS-16, and NASA GSFC NAG 5-3900 for visualization of earth science and DAO model data, NRA-97-MTPE-05, and RTOP 578-12-16-20 for IISS infrastructure and development.

References

- Dvorak, V. F., 1984: Tropical cyclone intensity analysis using satellite data. NOAA Tech. Memo. NES 11, 47 pp.
- Erikson, A., 1990: Use of cloud motion winds at ECMWF. *Proc. Eighth METEOSAT Scientific Users' Meeting*, Norrkoping, Sweden, EUMETSAT, EUMP 05, 79–86 [Available from EUMETSAT, Am Elfengrund 45, 6100 Darmstadt, Germany.]
- Fujita, T., D. L. Bradbury, C. Murino, and L. Mull, 1968: A study of mesoscale cloud motions computed from ATS-1 and terrestrial photographs from satellite. Mesometeorological Research Project Research Paper 71, Department of Geophysical Sciences, University of Chicago, 25 pp.
- Goerss, J. S., C. S. Velden, and J. D. Hawkins, 1998: The impact of multispectral GOES-8 wind information on Atlantic tropical cyclone track forecasts in 1995. Part II: NOGAPS forecasts. *Mon. Wea. Rev.*, **126**, 1219–1227.
- Hasler, A. F., 1970: Properties of tropical cloud clusters determined from geostationary satellite pictures. Annual Sci. Rep. NASS-11542, 1970–1971, Space Science and Engineering Center, University of Wisconsin, 166–270. [Available from Space Science and Engineering Center, University of Wisconsin, 1225 W. Dayton St., Madison, WI 53706.]
- , 1972: Properties of tropical cloud clusters determined from geostationary satellite pictures. Ph.D. dissertation, Dept. of Meteorology, University of Wisconsin, 317 pp. [Available from Space Science and Engineering Center, University of Wisconsin, 1225 W. Dayton St., Madison, WI 53706.]
- , and K. R. Morris, 1986: Hurricane structure and wind fields from stereoscopic and infrared satellite observations and radar data. *J. Climate Appl. Meteor.*, **25**, 709–727.
- , W. C. Skillman, W. E. Shenk, and J. Steranka, 1979: In situ aircraft verification of the quality of satellite cloud winds over oceanic regions. *J. Appl. Meteor.*, **18**, 1481–1489.
- , K. Palaniappan, M. Manyin, and J. Dodge, 1994: A high performance Interactive Image SpreadSheet (IISS). *Comput. Physics*, **8**, 325–342.
- Huang, Y., K. Palaniappan, X. Zhuang, and J. Cavanaugh, 1995: Optic flow field segmentation and motion estimation using a robust genetic partitioning algorithm. *IEEE Trans. Pattern Anal. Machine Intell.*, **17**, 1177–1190.
- Hubert, L. F., and L. F. Whitney Jr., 1971: Wind estimation from geostationary satellite pictures. *Mon. Wea. Rev.*, **99**, 665–672.
- Kambhamettu, C., K. Palaniappan, and A. F. Hasler, 1996: Automated cloud-drift winds from GOES images. *Proc. SPIE GOES-8 and Beyond*, Denver, CO, Int. Society for Optical Engineering, 122–133.
- Kidder, S. Q., and T. H. Vonder Haar, 1995: *Satellite Meteorology: An Introduction*. Academic Press, 466 pp.
- Leese, J. A., C. S. Novak, and B. B. Clark, 1971: An automated technique for obtaining cloud motion from geosynchronous satellite data using cross-correlation. *J. Appl. Meteor.*, **10**, 118–132.
- Menzel, W. P., and J. F. W. Purdom, 1994: Introducing GOES-I: The first of a new generation of geostationary operational environmental satellites. *Bull. Amer. Meteor. Soc.*, **75**, 757–781.
- Merrill, J., W. P. Menzel, W. Baker, J. Lynch, and E. Legg, 1991: A report on the recent demonstration of NOAA's upgraded capability to derive cloud motion satellite winds. *Bull. Amer. Meteor. Soc.*, **72**, 372–376.
- Nieman, S., W. P. Menzel, C. S. Velden, and S. Wanzong, 1996: Automated cloud-motion winds from GOES-8/9. *Proc. SPIE GOES-8 and Beyond*, Denver, CO, Int. Society for Optical Engineering, 60–67.
- Palaniappan, K., C. Kambhamettu, A. F. Hasler, and D. B. Goldgof, 1995: Structure and semi-fluid motion analysis of stereoscopic satellite images for cloud tracking. *Proc. Fifth Int. Conf. on Computer Vision*, Cambridge, MA, IEEE, 659–665.
- , M. Faisal, C. Kambhamettu, and A. F. Hasler, 1996: Implementation of an automatic semi-fluid motion analysis algorithm on a massively parallel implementation computer. *Proc. 10th IEEE Int. Parallel Processing Symp.*, Honolulu, HI, IEEE, 864–872.
- , J. Vass, and X. Zhuang, 1998: Parallel robust relaxation algorithm for automatic stereo analysis. *Proc. SPIE Parallel and Distributed Methods for Image Processing II*, San Diego, CA, Society for Photo-optical Instrumentation Engineers, in press.
- Phillips, D. R., E. A. Smith, and V. E. Suomi, 1972: Comments on "An automated technique for obtaining cloud motion from geosynchronous satellite data using cross correlation." *J. Appl. Meteor.*, **11**, 752–754.
- Press, W. H., S. A. Teukolsky, W. T. Vetterling, and B. P. Flannery, 1992: *Numerical Recipes in FORTRAN*. Cambridge University Press, 994 pp.
- Smith, E. A., and D. R. Phillips, 1972: Automated cloud tracking using precisely aligned digital ATS pictures. *IEEE Trans. Comput.*, **C-21**, 715–729.
- Velden, C. S., C. M. Hayden, W. P. Menzel, J. L. Franklin, and J. Lynch, 1992: The impact of satellite-derived winds on numerical hurricane track forecasting. *Wea. Forecasting*, **7**, 107–118.
- , —, S. J. Nieman, W. P. Menzel, S. Wanzong, and S. Goerss, 1997: Upper-tropospheric winds derived from geostationary satellite water vapor observations. *Bull. Amer. Meteor. Soc.*, **78**, 173–195.
- , T. Olander, and S. Wanzong, 1998: The impact of multispectral GOES-8 wind information on Atlantic tropical cyclone track forecasts in 1995. Part I: Dataset methodology, description, and case analysis. *Mon. Wea. Rev.*, **126**, 1202–1218.
- Young, M. T., R. C. Doolittle, and L. M. Mace, 1972: Operational procedures for estimating wind vectors from geostationary satellite data. NOAA Tech. Memo. NESS 39, NESDIS/NOAA, Washington, DC, 19 pp.

mature hurricanes than the Dvorak technique (Dvorak 1984) now in use.

Combining these measurements in the inner-core and eye regions with the cloud and water vapor derived winds of Velden et al. (1998) in the outer regions will give a much improved view of tropical cyclones over a wide range of spatial and temporal scales.

In addition to the unique long sequence of 1-min NOAA GOES images of Luis, many other datasets have been processed and coregistered. Those data include airborne weather radar, Doppler radar, and wind data from the NOAA WP-3D and AFRES WC-130 that were in the eye later in the day on 5 September 1995 around 1600 and 1900 UTC. Wind fields from the MPSMA automatic technique for the later periods have also been processed. There were a number of stronger convective outbursts later in the day. It will be interesting to see how these outbursts affect the winds at the tropopause in the CDO region. Studies relating satellite observations of the convective outbursts (cloud-top outburst morphology, CDO tropopause winds, low-level winds in the eye, GOES-8/9 stereo heights, etc.) to the WP-3D and WC-130 aircraft data are in progress. Mesoscale Model Version 5 (MM5) 3D numerical model simulations of Hurricane Luis on $22 \times 11 \times 3$ km nested-grid scales have also been run. Currently the model storm is too shallow. It does not accurately reflect the strong closed circulation revealed by the satellite-derived CDO tropopause winds. The convective parameterization and boundary layer schemes are being modified to see if a more realistic storm can be simulated that matches the in situ and satellite observations.

Viewing hurricane animation sequences with image intervals ranging from 1 to 30 min like those during Guillermo, see Fig. 14, is very disconcerting for lay persons and experts alike. Furthermore, even the long Luis 1-min image sequence has numerous gaps from 2 to 4 min. Until now the lapse-dissolve technique used for bridging these gaps has been much

less than satisfactory. A morphing technique similar to those commonly used for special effects on commercial television has been used very effectively to bridge gaps up to 30 min in the Guillermo sequence. Morphing shows great promise in making continuous sequences for science and public outreach. However, the morphing technique used to date is extremely labor intensive. Output of the robust automatic cloud feature matching technique described here is being used as input to an automatic morphing technique that could be used operationally.

The nearly continuous 12-h sequence of images from the NOAA GOES-9 satellite of Hurricane Luis on 6 September 1995 used in this study is the *only* long duration sequence at 1-min intervals that has ever been taken of a mature tropical cyclone (see Fig. 14). Figure 14 shows a comparison of the following: 1) the long 1-min image sequence taken during the Hurricane Luis GOES-9 test in 1995; 2) special short 1-min sequences of Hurricane Guillermo obtained during GOES-9 normal operations in 1997; and 3) 15-min data of Hurricane Linda in 1997. The 15-min data of Linda are all that was obtained this past year of the strongest storm ever observed in the eastern Pacific.

The authors believe that the techniques described in this paper have great potential for further research on tropical cyclones and severe weather as well as in operational use for nowcasting and forecasting. United States and foreign policymakers are urged to augment the GOES, Geostationary Meteorological Satellite, FY2 (Feng-Yun-2B), and Meteosat geostationary satellite systems with dual imaging systems such that 1-min observations are routinely taken.

Acknowledgments. The authors would like to acknowledge Matt Easton, now a graduate student of Bill Gray at CSU, for making the first estimates of Hurricane Luis CDO tropopause winds in a senior undergraduate paper. The authors had been looking at the CDO cloud structure motions since our first movies of Luis were made on 6 September 1995. The authors were not originally convinced that the motions were good estimators of the

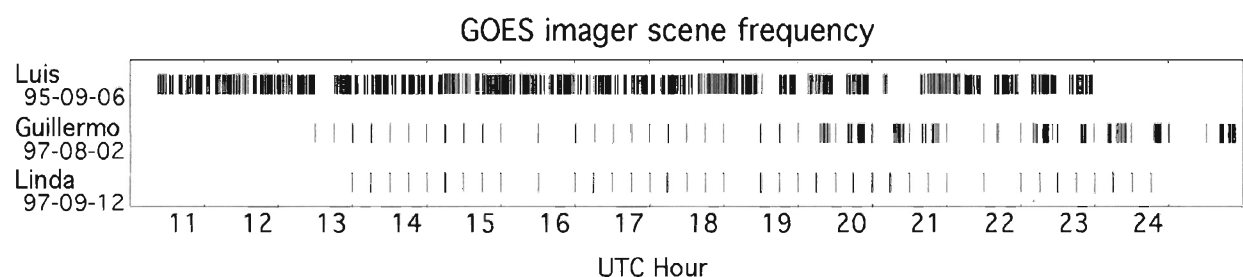


FIG. 14. NOAA GOES-9 image frequency for Hurricanes Luis, Guillermo, and Linda.

winds. However, once Matt Easton's results were presented and cloud tracks up to 90 min were obtained, it was apparent that an important new source of observations in mature hurricanes is at hand. Review of the manuscript with thoughtful suggestions by Mohan Karyampudi is greatly appreciated. The authors would like to thank Marit Jentoft-Nilsen and Hal Pierce for their work in processing the data for this study. The authors would also like to thank Jim Purdom and Joe Friday of NOAA for their support of the 1-min "rapid scan" NOAA GOES-9 operations. The development of the MPSMA automatic cloud tracking technique and IISS were supported under NASA grants, including NASA AISRP NRA-93-OSSA-09 for parallel motion analysis, NASA MTPE NRA-94-MTPE-02, NRA-94-OSS-16, and NASA GSFC NAG 5-3900 for visualization of earth science and DAO model data, NRA-97-MTPE-05, and RTOP 578-12-16-20 for IISS infrastructure and development.

References

- Dvorak, V. F., 1984: Tropical cyclone intensity analysis using satellite data. NOAA Tech. Memo. NES 11, 47 pp.
- Erikson, A., 1990: Use of cloud motion winds at ECMWF. *Proc. Eighth METEOSAT Scientific Users' Meeting*, Norrkoping, Sweden, EUMETSAT, EUMP 05, 79–86 [Available from EUMETSAT, Am Elfengrund 45, 6100 Darmstadt, Germany.]
- Fujita, T., D. L. Bradbury, C. Murino, and L. Mull, 1968: A study of mesoscale cloud motions computed from ATS-1 and terrestrial photographs from satellite. Mesometeorological Research Project Research Paper 71, Department of Geophysical Sciences, University of Chicago, 25 pp.
- Goerss, J. S., C. S. Velden, and J. D. Hawkins, 1998: The impact of multispectral GOES-8 wind information on Atlantic tropical cyclone track forecasts in 1995. Part II: NOGAPS forecasts. *Mon. Wea. Rev.*, **126**, 1219–1227.
- Hasler, A. F., 1970: Properties of tropical cloud clusters determined from geostationary satellite pictures. Annual Sci. Rep. NASS-11542, 1970–1971, Space Science and Engineering Center, University of Wisconsin, 166–270. [Available from Space Science and Engineering Center, University of Wisconsin, 1225 W. Dayton St., Madison, WI 53706.]
- , 1972: Properties of tropical cloud clusters determined from geostationary satellite pictures. Ph.D. dissertation, Dept. of Meteorology, University of Wisconsin, 317 pp. [Available from Space Science and Engineering Center, University of Wisconsin, 1225 W. Dayton St., Madison, WI 53706.]
- , and K. R. Morris, 1986: Hurricane structure and wind fields from stereoscopic and infrared satellite observations and radar data. *J. Climate Appl. Meteor.*, **25**, 709–727.
- , W. C. Skillman, W. E. Shenk, and J. Steranka, 1979: In situ aircraft verification of the quality of satellite cloud winds over oceanic regions. *J. Appl. Meteor.*, **18**, 1481–1489.
- , K. Palaniappan, M. Manyin, and J. Dodge, 1994: A high performance Interactive Image SpreadSheet (IISS). *Comput. Physics*, **8**, 325–342.
- Huang, Y., K. Palaniappan, X. Zhuang, and J. Cavanaugh, 1995: Optic flow field segmentation and motion estimation using a robust genetic partitioning algorithm. *IEEE Trans. Pattern Anal. Machine Intell.*, **17**, 1177–1190.
- Hubert, L. F., and L. F. Whitney Jr., 1971: Wind estimation from geostationary satellite pictures. *Mon. Wea. Rev.*, **99**, 665–672.
- Kambhamettu, C., K. Palaniappan, and A. F. Hasler, 1996: Automated cloud-drift winds from GOES images. *Proc. SPIE GOES-8 and Beyond*, Denver, CO, Int. Society for Optical Engineering, 122–133.
- Kidder, S. Q., and T. H. Vonder Haar, 1995: *Satellite Meteorology: An Introduction*. Academic Press, 466 pp.
- Leese, J. A., C. S. Novak, and B. B. Clark, 1971: An automated technique for obtaining cloud motion from geosynchronous satellite data using cross-correlation. *J. Appl. Meteor.*, **10**, 118–132.
- Menzel, W. P., and J. F. W. Purdom, 1994: Introducing GOES-I: The first of a new generation of geostationary operational environmental satellites. *Bull. Amer. Meteor. Soc.*, **75**, 757–781.
- Merrill, J., W. P. Menzel, W. Baker, J. Lynch, and E. Legg, 1991: A report on the recent demonstration of NOAA's upgraded capability to derive cloud motion satellite winds. *Bull. Amer. Meteor. Soc.*, **72**, 372–376.
- Nieman, S., W. P. Menzel, C. S. Velden, and S. Wanzong, 1996: Automated cloud-motion winds from GOES-8/9. *Proc. SPIE GOES-8 and Beyond*, Denver, CO, Int. Society for Optical Engineering, 60–67.
- Palaniappan, K., C. Kambhamettu, A. F. Hasler, and D. B. Goldgof, 1995: Structure and semi-fluid motion analysis of stereoscopic satellite images for cloud tracking. *Proc. Fifth Int. Conf. on Computer Vision*, Cambridge, MA, IEEE, 659–665.
- , M. Faisal, C. Kambhamettu, and A. F. Hasler, 1996: Implementation of an automatic semi-fluid motion analysis algorithm on a massively parallel implementation computer. *Proc. 10th IEEE Int. Parallel Processing Symp.*, Honolulu, HI, IEEE, 864–872.
- , J. Vass, and X. Zhuang, 1998: Parallel robust relaxation algorithm for automatic stereo analysis. *Proc. SPIE Parallel and Distributed Methods for Image Processing II*, San Diego, CA, Society for Photo-optical Instrumentation Engineers, in press.
- Phillips, D. R., E. A. Smith, and V. E. Suomi, 1972: Comments on "An automated technique for obtaining cloud motion from geosynchronous satellite data using cross correlation." *J. Appl. Meteor.*, **11**, 752–754.
- Press, W. H., S. A. Teukolsky, W. T. Vetterling, and B. P. Flannery, 1992: *Numerical Recipes in FORTRAN*. Cambridge University Press, 994 pp.
- Smith, E. A., and D. R. Phillips, 1972: Automated cloud tracking using precisely aligned digital ATS pictures. *IEEE Trans. Comput.*, **C-21**, 715–729.
- Velden, C. S., C. M. Hayden, W. P. Menzel, J. L. Franklin, and J. Lynch, 1992: The impact of satellite-derived winds on numerical hurricane track forecasting. *Wea. Forecasting*, **7**, 107–118.
- , —, S. J. Nieman, W. P. Menzel, S. Wanzong, and S. Goerss, 1997: Upper-tropospheric winds derived from geostationary satellite water vapor observations. *Bull. Amer. Meteor. Soc.*, **78**, 173–195.
- , T. Olander, and S. Wanzong, 1998: The impact of multispectral GOES-8 wind information on Atlantic tropical cyclone track forecasts in 1995. Part I: Dataset methodology, description, and case analysis. *Mon. Wea. Rev.*, **126**, 1202–1218.
- Young, M. T., R. C. Doolittle, and L. M. Mace, 1972: Operational procedures for estimating wind vectors from geostationary satellite data. NOAA Tech. Memo. NESS 39, NESDIS/NOAA, Washington, DC, 19 pp.